Applied Surface Science 488 (2019) 194–204

Contents lists available at ScienceDirect

Applied Surface Science

journal homepage: www.elsevier.com/locate/apsusc

Full length article

Anti-bacterial efficacy via drug-delivery system from layer-by-layer coating for percutaneous dental implant components

Erica D. de Avila[a,b,*], Antonio G.B. Castro[a], Oya Tagit[c], Bastiaan P. Krom[d], Dennis Löwik[e], Ad A. van Well[f], Lars J. Bannenberg[f], Carlos Eduardo Vergani[b], Jeroen J.J.P. van den Beucken[a,*]

[a] Regenerative Biomaterials, Radboudumc, Philips van Leydenlaan 25, Nijmegen, the Netherlands
[b] Department of Dental Materials and Prosthodontics, School of Dentistry at Araraquara, Sao Paulo State University (Unesp), Humaita, 1680 Araraquara, Sao Paulo, Brazil
[c] Department of Tumor Immunology, Radboudumc and Radboud Institute for Molecular Life Sciences (RIMLS), Geert Grooteplein Zuid, 28 Nijmegen, the Netherlands
[d] Department of Preventive Dentistry, Academic Centre for Dentistry Amsterdam (ACTA), University of Amsterdam and Vrije Universiteit Amsterdam, Gustav Mahlerlaan, 3004, Amsterdam, the Netherlands
[e] Department of Organic Chemistry, Radboud University, Heyendaalseweg 135, Nijmegen, the Netherlands
[f] Faculty of Applied Sciences, Delft University of Technology, Lorentzweg 1, Delft, the Netherlands

ARTICLE INFO

Keywords:
Surface modification
Layer-by-layer
Anti-bacterial
Porphyromonas gingivalis

ABSTRACT

Percutaneous medical devices are prone to bacterial contamination that causes dramatic clinical conditions. At the percutaneous level of dental implant systems, microbial pathogens induce biofilm formation that may result in bone resorption and dental implant loss. In view of peri-implantitis caused by bacterial inflammation at the percutaneous abutment region, we here establish a novel drug release system based on layer-by-layer (LbL)-deposited poly(acrylic acid) (PAA) and poly-L-lysine (PLL) coatings on titanium (Ti). Detailed multilayer coating characterization was performed by different microscopy and spectroscopy techniques to probe physical and chemical properties. Our data revealed a significant difference in roughness average between ten double layers coated (141 nm ± 30) and uncoated Ti discs (115 nm ± 40). Although roughness of the coatings increased significantly after immersion in water for 24 h at 37 °C, this physical property remained below 200 nm. Coating stability was confirmed under neutral and acidic pH, mimicking healthy and diseased/inflammatory environments, respectively. LbL coatings supported in vitro human keratinocytes growth, demonstrating absence of cytotoxic effects. Tetracycline (TC) showed an initial burst release under neutral and acidic conditions, which further demonstrated robust antibacterial efficacy against *Porphyromonas gingivalis*. However, a convenient pH-dependent 2-folds increase in TC release was observed for coatings incubated at pH = 4.5. Sustained TC release was observed from coatings up till 15 days of incubation in both pH conditions. These results demonstrate the potential application of this simple surface modification to leverage anti-bacterial efficacy at the percutaneous abutment region.

1. Introduction

Biofilm-based infections arise as the main cause of percutaneous implant loss after medical device implantation [1,2]. Microorganisms in the biofilm form are responsible for a substantial portion of healthcare-related infections. Over 65% of all human infections have been estimated to be biofilm-related [2]. Among several factors involved in infection progression, such as host response, presence of systemic disease and smoking habit [3], bacteria attached to material surfaces act as the major reason that infections are very difficult to eradicate [4]. As such, biofilm is a dreaded and organized biological structure developed by microorganisms growing on a surface and enclosed in an exopolysaccharide matrix [5]. Effective protection against antimicrobial substances provided by this matrix hinders the elimination of microorganisms and allows the infectious disease to diffuse further into tissue [6].

Particularly with percutaneous devices (PDs), the oral mucosa/skin-implant interface (initially) does not totally seal the internal environment, which may facilitate pathogen invasion to the body. For dental implants, a polymicrobial biofilm infection might lead to inflammation of tissues surrounding the implant, eventually resulting in progressive bone resorption [7,8]. Under healthy conditions, oral mucosal cells

* Corresponding authors at: Regenerative Biomaterials (309), Radboudumc, Philips van Leijdenln 25, 6525EX Nijmegen, the Netherlands.
E-mail addresses: erica.fobusp@yahoo.com.br, erica.foar@gmail.com (E.D. de Avila), jeroen.vandenbeucken@radboudumc.nl (J.J.J.P. van den Beucken).

https://doi.org/10.1016/j.apsusc.2019.05.154
Received 7 December 2018; Received in revised form 18 April 2019; Accepted 14 May 2019
Available online 15 May 2019
0169-4332/

work as a physical barrier against the invasion of microorganisms and only a small number of bacterial species can reach the internal environment [9]. However, once peri-implantitis has established, a high number of bacteria from the infected oral site can gain access into the internal environment and reach vital organs, including as lung, heart and the peripheral blood capillary system [10]. The broad and well-documented knowledge about the dramatic complications involving implant-related infection [11] has awakened clinicians and engineers to search for new strategies to combat biofilm-associated diseases.

Since oral microorganisms adhere to generally all types of substrates [12–17], material engineers developing next generation oral care products are progressively developing new materials and material surface modifications that reduce bacterial attachment to titanium (Ti) implants [18]. One of the main engineering challenges in biotechnology and nanomedicine is the development of a surficial drug release system to attain anti-bacterial activity without cytotoxicity concerns [19]. Several metallic nanoparticle films have been developed in an attempt to limit the growth of bacteria [20,21]. However, the main disadvantage related to the clinical application of metallic nanoparticles is the potential health risk owing to toxicity and (nano)particle accumulation [22–24].

Currently, the development of surficial drug-delivery systems for antibacterial agents has attracted attention as an effective approach to prevent and treat implant-related infections [25–27]. Among the explored coating techniques, layer-by-layer (LbL) self-assembly based on polyelectrolyte deposition via electrostatic interactions has shown biological advantages, including precise control of coating properties, low-cost built-up, versatility for coating any available surface, obtainment of homogeneous films with controlled thickness, and incorporation and controlled release of biomolecules/drugs [28–30]. The ability of LbL systems to incorporate drugs in different amounts and the versatile chemical properties within a thin film render the method appealing. In brief, LbL exploits interactions between oppositely charged polyelectrolytes to obtain a layered coating [31]. The intermolecular interaction between moieties within the coating (i.e. polyelectrolytes and drugs) depends on the size and overall charge density [32,33].

With Ti-based dental implant components as a key site for biofilm formation, we here demonstrate a novel drug release system based on LbL-deposited poly(acrylic acid) (PAA) and poly-L-lysine (PLL) coatings as a model for surficial anti-bacterial efficacy using tetracycline as an antibiotic. We characterized LbL-deposited coatings in detail using multiple advanced microscopy and spectroscopy techniques to probe physical and chemical coating properties. Stability assessment of the coatings was evaluated under different pH conditions mimicking healthy and diseased/inflammatory environments [34,35]. Furthermore, tetracycline was incorporated within the LbL coating and bacteriostatic effects were tested on mono-species early biofilms. Concomitantly, cytotoxicity of the surface modification was tested using human keratinocytes.

2. Material and methods

2.1. Titanium discs, materials and reagents preparation

Commercially pure titanium (Ti; Grade 2), machined discs (12 mm diameter, 1.5 mm thickness) were obtained from Machinefabriek G Janssen B.V. (Valkenswaard, the Netherlands). Polyethylenimine (PEI) (M.W. = 25,000), poly-L-lysine FITC Labeled (PLL) (M.W. = 15,000–30,000), tetracycline hydrochloride (TC), UltraPure™ Tris buffer (≥99.9%) and sodium acetate (M.W. = 82.03) were purchased from Sigma-Aldrich (St. Louis, MO, USA). Poly(acrylic acid) (PAA; M.W. = 60,000) and sodium chloride for analysis were obtained from Polysciences (Warrington, PA, USA) and Millipore Corporation (Burlington, MA, USA), respectively.

2.2. LbL coating assembly

Prior to LbL coating assembly, Ti discs were cleaned with acetone for 15 min in ultrasound, followed by a wash-step with Milli-Q water for 15 min in ultrasound, and 2-propanol for 10 min. Discs were then air-dried at room temperature (RT) for 24 h. To functionalize the surface, Ti discs were plasma-etched in argon using plasma cleaner machine (PDC-002, Harrick Scientific Corp., NY, USA) for 5 min. Immediately after plasma-etching, LbL coatings were assembled using the LbL assembly following method: First, the build-up of the coating was initiated by immersing the Ti disc in a PEI solution (0.5% w/v PEI in 10 mM Tris buffer containing 150 mM sodium chloride; pH = 7.4) for 30 min. Thereafter, alternating PAA (1 mg/mL in a 150 mM sodium chloride solution; pH = 5.5) and PLL (1 mg/mL in 10 mM of Tris buffer containing 150 mM of sodium chloride; pH = 7.4) immersion steps (each 10 min) with intermediate washing steps in Milli-Q water (1 min) were used to reach a $[PAA/PLL]_n$ system (n ranging from 5 to 10).

2.3. LbL coating characterization

LbL coatings were deposited on Ti discs displaying a standard roughness surface lower than 200 nm. However, to determine the thickness of the multilayer system and evaluate the effect of the temperature and immersion solution on the roughness of the polyelectrolytes coatings, [PAA/PLL]n coatings were deposited onto silicon wafer with Ti-coating as flat substrates [36].

2.3.1. Fluorescence microscope

The build-up of coatings was monitored by measuring the fluorescence intensity of PLL-FITC from $[PAA/PLL]_5$ and $[PAA/PLL]_{10}$ (EL 6000 Fiber Optic Illuminator, Leica Microsystems CMS, Wetzlar, Germany). LbL coating assembly was carried out at room temperature and coated Ti discs were stored in the dark at room temperature.

2.3.2. Atomic force microscopy (AFM)

2.3.2.1. Surface roughness analyze. Atomic force microscopy (AFM) measurement was performed to determine the average roughness (Ra) of coated and uncoated Ti discs. Images were taken at 300 kHz using silicon nitride cantilevers (RTESP-300, Bruker, Bremen, Germany). Surface roughness calculations from scan size of 20 × 20 μm were averaged over five separate areas for coated and uncoated Ti discs.

2.3.2.2. Substrate preparation for atomic force microscopy imaging. AFM imaging was performed to determine the surface profile and thickness of coating. To avoid effects of irregular surface topography of Ti discs, we assembled $[PAA/PLL]_n$ coatings on Ti-coated silicon wafers (12 × 12 mm). This Ti coating was deposited using physical vapor deposition (Auto 500, HHV Ltd., West Sussex, UK) and a high purity Ti target in a static modus for 45 min. The presence of a thin TiO_2 layer on the silicon wafer was confirmed by field emission scanning electron microscopy (FESEM - JEOL, 6330 Cryo, MA, USA) combined with energy dispersive spectroscopy (EDS), as well as Neutron Reflectometry [37], see below, and X-ray Diffraction (XRD) (Cu-Kα, 40 kV, X'Pert, PANalytical, Almelo, the Netherlands). LbL deposition of coating on this substrate was achieved following the same sequence described above (Section 2.2; Fig. 1).

2.3.2.3. Atomic force microscopy imaging. Atomic force microscopy images were obtained with a Catalyst BioScope (Bruker, Bremen, Germany) coupled to a confocal microscope (TCS SP5II, Leica, Mannheim, Germany). 10 × 10 μm regions of [PAA/PLL] coating Ti discs with 5 and 10 double layers were imaged in tapping mode using silicon nitride cantilevers with nominal resonant frequency of 300 kHz (RTESP-300, Bruker, Bremen, Germany). In order to evaluate the thickness of the coating, two different regions of each disc were scratched with ethanol and the distance from the Ti surface was

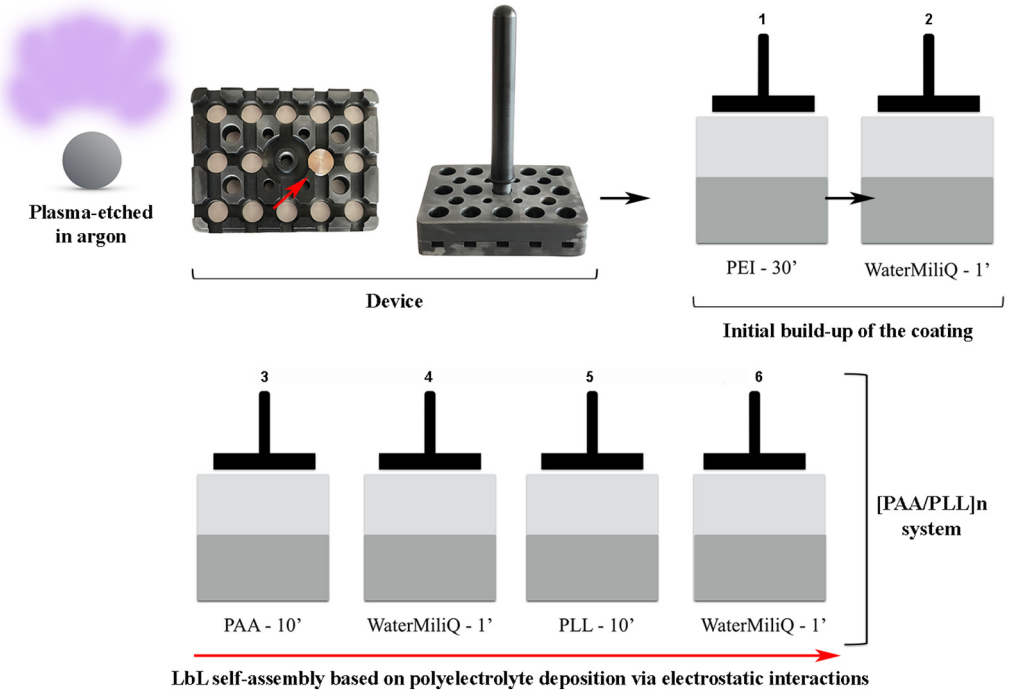

Fig. 1. Schematic illustration describing LbL self-assembly based on polyelectrolyte deposition.

measured using the NanoScope software (Bruker, Bremen, Germany). Root mean square values were determined using the roughness feature of the NanoScope software as well.

2.3.3. Confocal laser scanning microscopy (CLSM)

Ti discs with coatings, for which PLL-FITC was used during LbL coating assembly, were subjected to CLSM, acquiring digital images in the green channel of a CLSM (Olympus FV1000, Inverted, Tokyo, Japan) with an excitation wavelength of 488 nm. Three random regions of each coated Ti disc were analyzed and the data plotted as mean of green fluorescence.

2.3.4. X-ray photoelectron spectroscopy (XPS)

Surface elemental composition of coating was determined by quantitative X-ray photoelectron spectroscopy (XPS) on a VG Scientific ESCALAB 200A spectrometer utilizing a non-mono-chromatized Al-Kα radiation (900 kV). A wide survey scans of 300 µm × 700 µm were performed in 2 different areas of two independent discs. Data analysis was processed with commercially available software (CasaXPS, Casa Software, Ltd., Cheshire, UK) and carbon 1s (C), nitrogen 1s (N), oxygen 1s (O), sulfur 2p (S) and titanium 2p (Ti) were quantified by integration of the significant intensity of photoelectron peaks. Uncoated Ti discs served as control.

2.3.5. Neutron reflectometry [37]

In order to complement our previous analyses and gain a more reliable understanding about the coating thickness, the coated and uncoated Ti discs were subjected to NR analyses. With NR, the reflectivity of neutrons is measured as a function of momentum transfer $Q = (4\pi/\lambda)\sin(\theta)$, with λ and θ the incident wavelength and angle of the neutron, respectively. By fitting these data to a scattering length density profile, one obtains estimates for thickness, roughness and scattering length density (SLD) of each layer. The SLD is a material property and equals the sum of the product of the atomic number density N_i and the isotope-dependent scattering length b_i product of each isotope in the layer, i.e., $SLD = \sum_i N_i b_i \mathrm{SLD} = \sum_{i=1}^{P} \mathrm{N_i b_i}$. The SLD thus depends on the density of the layer and the (ratio of) isotopes present in the material.

The NR measurements were performed using a time-of-flight ROG reflectometer as described previously [38] using neutrons with an incident wavelength of $0.17 < \lambda < 0.99$ nm, an incident angle of $\theta = 5.5$ and 9.1 mrad, and a momentum transfer resolution of $\Delta Q/Q = 0.04$. The neutron reflectometry measurements were fitted using the software package STAR (see [39] for more details) to obtain estimates for layer thickness, roughness and SLD for each layer.

2.4. In vitro LbL coating stability assessment

The fluorescence intensity, roughness and chemical composition variations of coating were evaluated before and after immersion in solutions with different pH. Discs were gently placed into 15 mL tubes containing 3 mL of PBS (pH 7.4) or acetate buffer (pH 4.5) [40] and incubated at 37 °C in shaking condition (60 rpm/min) for 15 days. The buffer solutions were refreshed daily. At retrieval, coated discs were rinsed once with Milli-Q water) jkm,r and the integrity of coatings was evaluated by CLSM, AFM and XPS, as described above (see Section 2.3).

2.5. MIC and MBC determination for tetracycline

Porphyromonas gingivalis ATCC W83 was initially grown anaerobically on brain heart infusion (BHI) blood agar with hemin and menadione for 5 days at 37 °C. Bacterial colonies were transferred to BHI broth medium supplemented with hemin and menadione (BHI-HM) and incubated at 37 °C under anaerobic conditions. *P. gingivalis* was used to inoculate 96-well microliter plates (Corning Costar cell culture plates; Fisher Scientific, NY, USA) to a final bacterial density of 10^9 CFU/mL containing two-fold serial dilution of TC in BHI-HM. The cultures were incubated at 37 °C under anaerobic conditions and the absorbance at OD_{600nm} was read after 48 h. The lowest concentrations of TC that inhibited *P. gingivalis* growth were plated and the number of viable bacteria determined the minimal bactericidal concentration (MBC). MBC represented our reference concentration to calculate the amount of antibiotic to be incorporated into coating.

2.6. Preparation of tetracycline-loaded coatings

Due to instability in air and light-sensitivity, TC was prepared immediately before each experiment. Drug incorporation method was outlined considering its dissociation constant (pKa) as a strategic physicochemical parameter to improve the electrostatic interaction between TC and polyelectrolytes. Briefly, 5 mg/mL of TC solution was prepared in Milli-Q water at room temperature. Then, 100 µL of this cationic drug was gently dropped on the last layer, after PLL deposition being completed, and discs were statically incubated at 37 °C for 4 days, in dark environment ($[PAA/PLL]_{10}$/TC). In an attempt to validate LbL assembly role on TC incorporation, 100 µL of TC at 5 mg/mL was pipetted on Ti discs that had not undergone coating for comparison. Concurrently, to confirm the effect of temperature on TC yield under multilayers, we dropped the same drug concentration after PLL deposition in ninth multilayer and followed with the last double layer construction ($[PAA/PLL]_9$ / TC + $[PAA/PLL]_1$) after incubation for 24 h at 37 °C.

2.7. Tetracycline release

TC release from the coating was monitored in two different pH conditions. Three $[PAA/PLL]_{10}$/TC coating Ti discs were placed into a 24-well plate containing 1 mL of PBS (pH = 7.4) and acetate buffer (pH = 4.5) and kept at 37 °C in shaking (60 rpm/min) for 1, 3, 7 and 15 days. At different sampling intervals, 1 mL of supernatant was collected for analysis and a fresh solution was added into each experimental well. Coated and uncoated Ti discs were used as controls. To determine the method detection limit, TC standard solutions were prepared in both PBS and acetate buffers, in the concentration range between 0.5 and 250 µg/mL. The PBS and acetate supernatant containing released tetracycline were analyzed by High-performance liquid chromatography machine (HPLC - Hitachi, Mannheim, Germany) consisting of a pump (Hitachi L-2130), a UV detector (Hitachi L-2400), an autosampler (Hitachi L-2200) and a LiChrospher RP-18 endcapped HPLC column (125 × 4 mm, particle size 5 µm). The flow rate of mobile phase (ammonia phosphate buffer 50 mM, pH 3, and acetonitrile 90/10 volume ratio) was fixed at 1 mL/min with an injection volume of 30 µL.

2.8. Biological assays

Before proceeding with biological experiments, Ti discs were sterilized in autoclave at 121 °C for 15 min. For LbL assembly preparation, all experimental solutions were filtered with a Millipore® membrane 0.22-µm-pore size filters and the complete LbL assembly was performed under aseptic conditions, inside a biosafety cabinet.

2.8.1. Antibacterial assay

$[PAA/PLL]_{10}$/TC coating Ti discs were placed in a 24-well culture plate (Corning Costar cell culture plates; Fisher Scientific, NY, USA) and incubated with 1 mL of *P. gingivalis* W83 in BHI-HM (supplemented with 25% filtered saliva), in the working density of approximately 10^9 CFU/mL under anaerobic conditions. After 48 h [41], PBS-washed coated and uncoated Ti discs were transferred to a new plate containing BHI broth medium and bacterial cells were harvested from the discs by scraping with a pipette tip. Two hundred µL of bacterial culture was transferred to a 96-well plate to serial dilution procedure. Ten µL of each sampling well was dropped on a fresh BHI blood agar plate and kept at 37 °C under anaerobic conditions. Viable colonies were counted after 5 days. Coated and uncoated Ti discs were used as controls. Concomitantly, *P. gingivalis* at the same sampling concentration were inoculated directly into the polystyrene well plate to serve as our positive control.

2.8.2. Cytotoxicity assay and cell viability experiments

HaCaT immortalized human keratinocytes were cultured in Dulbecco's Modified Eagle's Medium High Glucose (DMEM, Sigma Chemical Co., St. Louis, MO, USA) medium, supplemented with 10% fetal bovine serum (FBS, Gibco, Grand Island, NY, USA), 1% penicillin/streptomycin (Sigma-Aldrich, St. Louis, MO, USA), in a humidified atmosphere containing 5% CO_2 at 37 °C. The medium was refreshed every 48 h. Assessment of coating effects on metabolic mitochondrial activity of cells was performed by alamar blue assay. HaCat cells were seeded on the coated and uncoated Ti discs in 24-well culture plate (Greiner Bio-One, Kremsmünster, Austria) at 2×10^5 cells/well for monolayer cell culture. Coated and uncoated Ti discs were statically incubated at 37 °C under 5%CO_2 conditions for 24 h. After the incubation period, the medium was refreshed with 0.1 g/mL of alamar blue (Invitrogen, CA, USA) and the reduction of the non-fluorescent reagent (resazurin) to a fluorescent compound (resarufin) was read using a spectrophotometer (Synergy™ HTX Multi-Mode Microplate Reader, BioTek, Baden-Württemberg, Germany) at 570 nm and 600 nm wavelength. Cells from the same original culture growth on a 24-well polystyrene and DMEM medium served as positive and negative control respectively. The experiment was performed in triplicate and with two independent biological repetitions.

Cell viability was confirmed via a Calcein AM/ethidium homodimer-1 live/dead kit (Invitrogen, CA, USA), following manufacturer's instructions. The experiment was carried out 3 days post-seeding. Images from adhered cells on coated and uncoated Ti discs were acquired using a 20× dry objective on an inverted confocal microscope (Olympus FV1000, Japan). Excitation wavelengths of 488 and 543 nm lasers were employed in combination with bandpass filters of 505e530 nm and long-pass filter of 560 nm to demonstrate the live dead cells distribution.

Assessment of TC released from the $[PAA/PLL]_{10}$ coating Ti discs effects on metabolic mitochondrial activity of cells was also performed by alamar blue assay. For this, HaCat cells were seeded onto 24-well polystyrene plates at 2×10^5 cells/well and then the plates were incubated at 37 °C under 5% CO_2 conditions for 24 h, for monolayer cell culture formation. At the end of incubation period, TC was added into each correspondent well in different concentrations of 50 µg/mL, 100 µg/mL and 500 µg/mL with 10% alamarBlue (Invitrogen, Carlsbad, CA, USA). Longer incubation times at 24 and 72 h were established for greater cytotoxicity analyses.

2.9. Statistical data analysis

The normal and homoscedastic distribution of the data outlined parametric tests. Statistical comparisons were performed by one-way analysis of variance (ANOVA) with a Tukey's Post Hoc test. For evaluation of roughness between coated and uncoated Ti discs and liquid immersion and temperature on multilayer roughness, D'Agostino & Pearson was applied to test data distributions for normality and a paired Student's *t*-test (two-tailed) was employed using GraphPad Prism version 5.0c (GraphPad Software, CA, USA). All data were plotted as the mean ± standard deviation (SD) and $p < 0.05$ was considered statistically significant.

3. Results and discussion

3.1. Development and characterization of [PAA/PLL]n coatings on Ti surfaces

In this study, we demonstrated the successful implementation of an LbL system on Ti surfaces by alternate electrostatic interactions of alternating polyanions and polycations to fight *P. gingivalis* as a potential pathogen involved in oral diseases. The engineered LbL construction was generated after initial pre-treatment of Ti with ionized argon gas. This is an important step to improve electrostatic interaction between Ti substrate and PEI, a hydrophilic polyelectrolyte material. Ti discloses hydrophobic properties conferred by a natural and constant

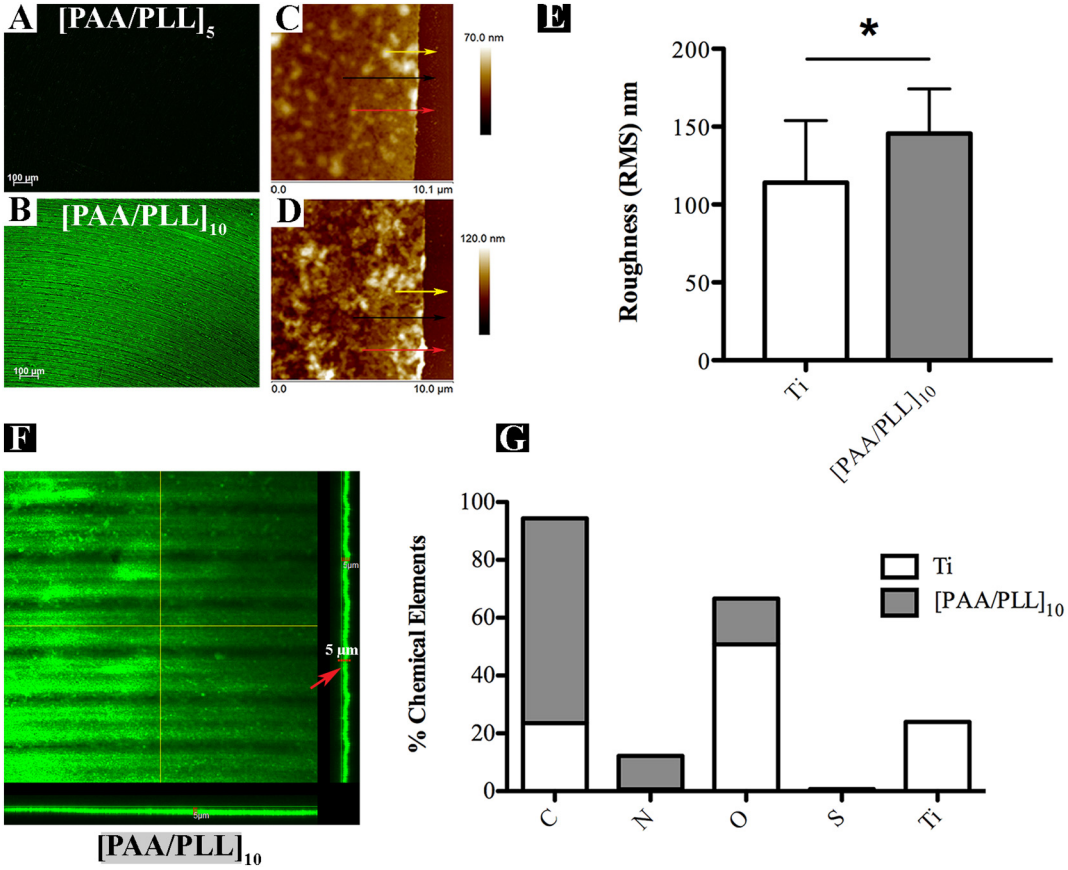

Fig. 2. LbL build-up on Ti discs was confirmed via fluorescence microscopy using FITC-labeled PLL for (A) $[PAA/PLL]_5$ and (B) $[PAA/PLL]_{10}$. Quantitative comparison of coating thickness between (C) $[PAA/PLL]_5$ and (D) $[PAA/PLL]_{10}$. Red, black and yellow arrows indicate the thickness measurement of different regions. (E) Surface roughness analysis of Ti and $[PAA/PLL]_{10}$ coating measured by AFM (*$p = 0.0249$). (F) Confocal microscopy reveals homogenous distribution of $[PAA/PLL]_{10}$ coating on Ti discs. The fluorescent bands suggest the top outlines of the polyelectrolytes coating thickness (arrow red). (G) Quantitative comparison between chemical composition of $[PAA/PLL]_{10}$ coating on Ti discs (gray bar-$[PAA/PLL]_{10}$) and uncoated Ti discs (white bar-Ti). The results show that the Ti discs was covered by a TiO_2 layer.

polycarbonyls and hydrocarbons deposition. This phenomenon affects the wettability of the surface with the increased hydrophobicity [42,43]. Our data confirmed the previous findings showing average contact angle values of 90 ± 2 degrees. Non-thermal plasma activation [37] modified Ti physical chemical properties from hydrophobic to superhydrophilic (2.1 ± 0.3).

Subsequent PEI immersion promoted cationic polyelectrolyte adherence, which was the basis for interaction with negatively charged PAA [44]. First [PAA/PLL] double layers were completed by a strong electrostatic interaction between dissociated carboxyl groups from PAA and extend primary amine groups of lysine residues in PLL. Since PAA and PLL are considered weak polyelectrolytes, the pH of the polyelectrolyte solutions is important [45]; this parameter was fixed at pH 5.5 for NaCl solution and pH 7.4 for Tris/NaCl buffer during deposition of stable double layer coatings. Five ($[PAA/PLL]_5$ - Fig. 2A) and ten double layers ($[PAA/PLL]_{10}$ - Fig. 2B) coating Ti discs were prepared and the fluorescence intensity originating from PLL-FITC layers revealed that $[PAA/PLL]_{10}$ was sufficient to homogeneously cover the surface of Ti discs.

In order to gain a better understanding on multilayer thickness, we measured the distance from Ti substrate to outer coating by AFM. Cross-section analysis of $[PAA/PLL]_5$ (Fig. 2C) and $[PAA/PLL]_{10}$ (Fig. 2D) on Ti-coated Si showed an average thickness of 20 nm and 40 nm, respectively.

A high density of irregularities, as well as the presence of considerable roughness, can facilitate bacterial accumulation on materials [46–48]. It has been reported that a threshold roughness value lower than 200 nm does not further affect the number of microorganisms adhered onto a material substrate [46–48]. Although our data revealed a significant difference in Ra between coated (Ra = 141 nm ± 30) and uncoated Ti discs (Ra = 115 nm ± 40; Fig. 2E), the overall peak-to-valley height obtained from both coated and uncoated Ti discs were fabricated according to the roughness standards indicated to implant confection, around 200 nm [46,47].

We further acquired CLSM images to estimate the fluorescent intensity scales with the thickness/amount of PLL-FITC labeled. In addition, we obtained information about the homogeneity and stability of the polymeric layers. $[PAA/PLL]_{10}$ revealed a homogeneous multilayer deposition on the Ti discs, with a consistent fluorescence intensity to all discs analyzed (Fig. 2F).

The wide scan spectrum of XPS (Fig. 1G) showed predominance of carbon (C) and nitrogen (N), and a small percentage of sulfur (S) at the surface of coatings. C content was increased on multilayer coating Ti discs due to the more C on molecular structure composition of polyelectrolytes used on LbL construction. The presence of N and S was directly attributed to the PLL-FITC.

Coating thickness is critical in the controlled processing and quality assessment for drug delivery [49,50]. Consequently, we used NR to further validate the previous findings and provide accurate information about $[PAA/PLL]_5$ thickness. In addition, we measured a separate silicon wafer and a silicon wafer with a TiO_2 layer (Fig. 3A). From the fits of these measurements, we deduce a TiO_2 layer thickness of 32.6 ± 0.9 nm and for the 5 double layers of the LbL coatings of 20.5 ± 0.8 nm (Fig. 3B). Assuming a constant layer thickness per

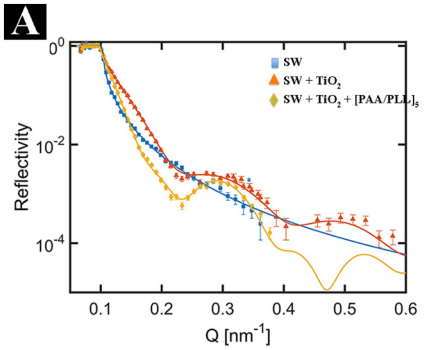

B

		SW	SW + TiO_2	SW + TiO_2 + $[PAA/PLL]_5$	Literature Value
SW	SLD [10^{-4} nm^{-2}]	2.1	2.1	2.1	2.07
TiO_2	d [nm]		31.7(7)	32.6(9)	
	SLD [10^{-4} nm^{-2}]		2.7	2.6	2.60
	σ [nm]		0.1	0.4	
$[PAA/PLL]_5$	d [nm]			20.5(8)	
	SLD [10^{-4} nm^{-2}]			1.1	1.41
	σ [nm]			2	

Fig. 3. (A) Neutron Reflectometry measurements of a Silicon Wafer (SW), SW with a TiO_2 layer and a SW with a TiO2 and -$[PAA/PLL]_5$ layer. The continuous lines indicate fits to the experimental data. (B) Estimates of the Scattering Length Density (SLD), thickness *d*, and roughness *σ* obtained by fitting the neutron reflectometry data of (A). The corresponding literature values of the SLD are included as a reference, where for the -$[PAA/PLL]_5$ layer an equal ratio of PAA ($1.76\ 10^{-4}\ nm^{-2}$)/PLL ($1.13\ 10^{-4}\ nm^{-2}$) was assumed.

double layer, this would translate to a double layer thickness of 40.8 nm for a 10 double layer system, which is in excellent agreement with AFM measurement that show a layer thickness of around 40 nm. The fitted scattering length density of the TiO_2 ($2.6 \cdot 10^{-4}\ nm^{-2}$) matches the literature value ($2.6 \cdot 10^{-4}\ nm^{-2}$), while the SLD of the $[PAA/PLL]_5$ coating was slightly lower than expected based on an equal ratio of PAA and PLL, possibly due to the inclusion of H_2O and/or HBr, which have a strong, negative effect on the scattering length density due to the negative scattering length of hydrogen. The atomic (local) roughness of the $[PAA/PLL]_5$ layer is approximately 2 nm.

3.2. Coating stability test in different pH conditions

Since coating stability is important for clinical applications, we examined if different pH conditions affect the coating surface properties over time. Fresh PBS (pH = 7.4) and acetate buffer (pH = 4.5) were prepared to simulate a normal and inflammatory environment, respectively. Sodium acetate is considered a stable buffer routinely used in biochemical studies to prevent pH changes of compounds involved in the biochemical activity [40]. CLSM analyses were performed to compare the homogeneity stability of the coating before and after immersion in different pH conditions. The results showed that neutral pH did not affect the green fluorescent signal after 15 days of incubations (Fig. 4B) compared to non-immersed coating Ti discs (Fig. 4A). In contrast, a notable difference in overall fluorescence intensity after coatings incubation for 15 days at acidic pH (Fig. 4C) was observed. Since it has been reported that fluorescein derivate from PLL-FITC is very sensitive to changes in pH and not very stable to elevated temperatures [51], photobleaching is expected after coatings incubated under acidic pH at 37 °C. Therefore, a possible interference of pH on PLL-FITC required additional investigation to improve understanding of the true effect of acidic environment on LbL coating stability.

XPS analyses indicated that exposure of the coatings to neutral and acidic pH hardly affected the amount of carbon (C), nitrogen (N), oxygen (O) and sulfur (S) compared to non-immersed coatings (Fig. 4D). Not measuring Ti (i.e. the underlying substrate) upon immersion in either pH conditions further confirms negligible coating degradation. Because PAA is known to have a very high liquid retention capacity [52], we assumed that molecular conformation change upon immersion caused a subsequent swelling behavior of the polyelectrolyte matrices. The swelling response is a consequence of liquid adsorption and ionic strength among polyelectrolyte layers and liquid, which can contribute to increased surface irregularity, and hence roughness of the coating. LbL coating showed significantly decreased values of roughness upon immersion (Fig. 4E), suggesting a deswelling response in dry environment [53].

We also found that the swelling property was maintained when roughness analyses were performed with coating Ti discs in an aqueous environment. This assumption was confirmed by AFM analyses. Roughness of the coatings on Ti-coated Si increased significantly after immersion in water (W) for 24 h at 37 °C (Fig. 5). Importantly, roughness values always remained below 200 nm, independent of

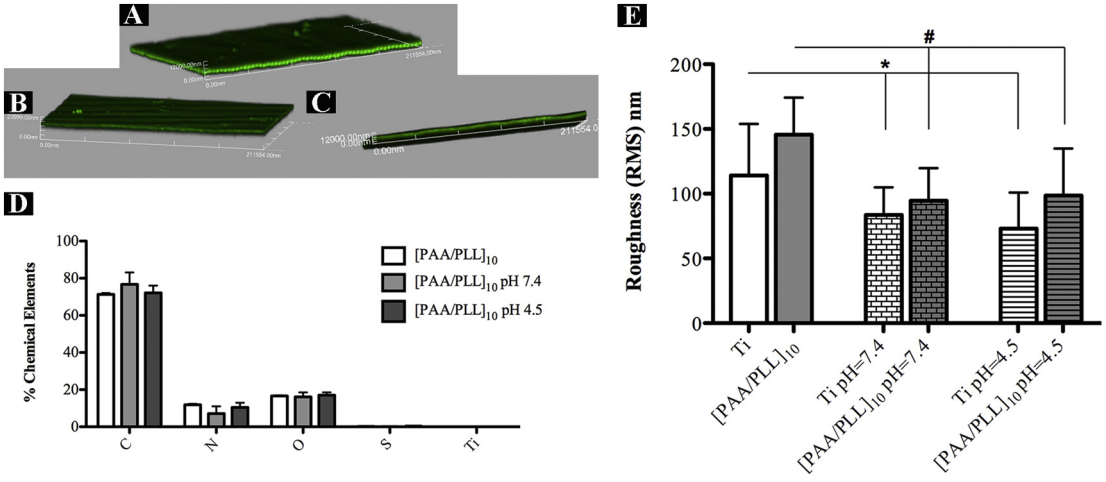

Fig. 4. (A) $[PAA/PLL]_{10}$ coated Ti without immersion. Effect of (B) pH 7.4 and (C) pH 4.5 on amount of green fluorescence from FITC-labeled PLL in the $[PAA/PLL]_{10}$ coatings. (D) Effect of pH 7.4 and pH 4.5 on $[PAA/PLL]_{10}$ coating chemical composition. (E) Effect of pH 7.4 and 4.5 on $[PAA/PLL]_{10}$ roughness. Data are shown as the mean ± SD. Statistically significant differences are indicated as: $p < 0.05$ ($^{*,\#}p < 0.0001$).

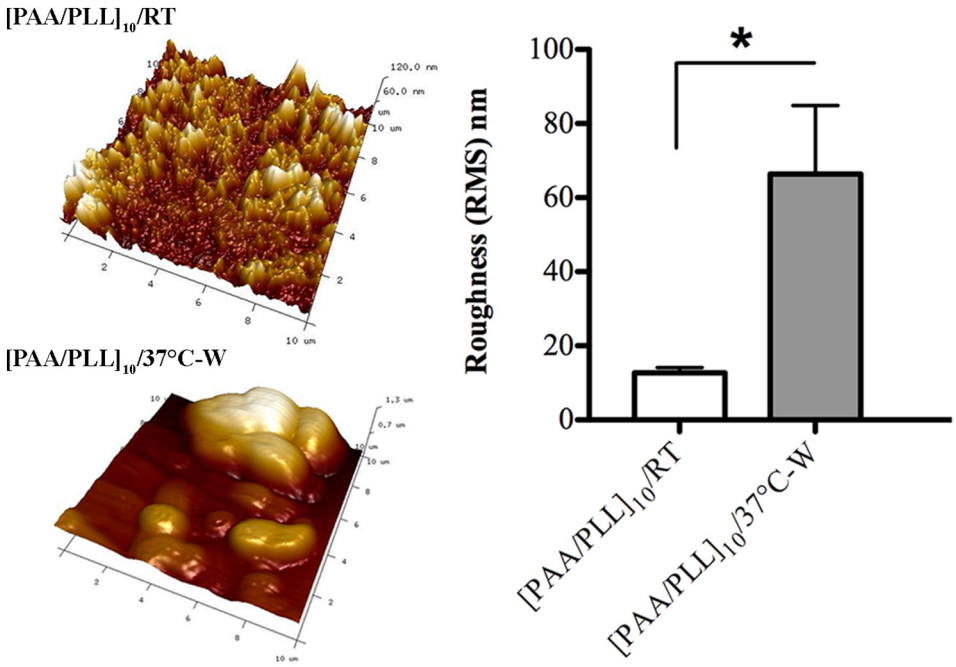

Fig. 5. Effect of immersion solution on roughness of $[PAA/PLL]_{10}$ on Ti coated Si (gray bar, $[PAA/PLL]_{10}$/37 °C-W) in comparison to $[PAA/PLL]_{10}$ (white bar, $[PAA/PLL]_{10}$/RT). Data are shown as mean ± SD. Statistically significant differences are indicated as: $p < 0.05$ (*$p < 0.0001$).

temperature and acidity.

3.3. Temperature facilitates TC incorporation within coatings

Altering polyelectrolytes structure can largely affect the hydrophilic/hydrophobic balance and hence polyelectrolyte/drug interactions [54]. Fig. 6A schematically illustrates coating conformation changes and the drug diffusion process through the multilayered LbL coating. To facilitate TC loading into the polyelectrolyte matrices, we placed a droplet of TC solution onto the coating at 37 °C for 4 days to produce $[PAA/PLL]_{10}$/TC with TC penetrating into the LbL-system. To validate the carrier role of coating, we also placed a droplet of TC on uncoated Ti discs and compared TC fluorescent intensity after 24 h of coating immersion in PBS. Fig. 6B and C show similarity in detection of the fluorescent signal from both pristine $[PAA/PLL]_{10}$/TC and Ti/TC. However, TC was easily released from Ti/TC after immersion in PBS (Fig. 6D), indicating limited interactions between the Ti substrate and TC. Interactions of coating with TC incorporation were confirmed by fluorescent signal emitted from TC after 24 h under different pH conditions (Figs. 6E-F). As drug loading often relies on diffusive processes controlled by LbL internal structure properties [30,55], our stability data suggests clear interactions at room temperature between both polyelectrolytes used for LbL-coating build-up. Then, a last experiment was performed in an attempt to ensure temperature as a crucial property to improve drug loading through the layers. Here, TC was dropped on the ninth multilayer constructed and kept at 37 °C for 24 h before

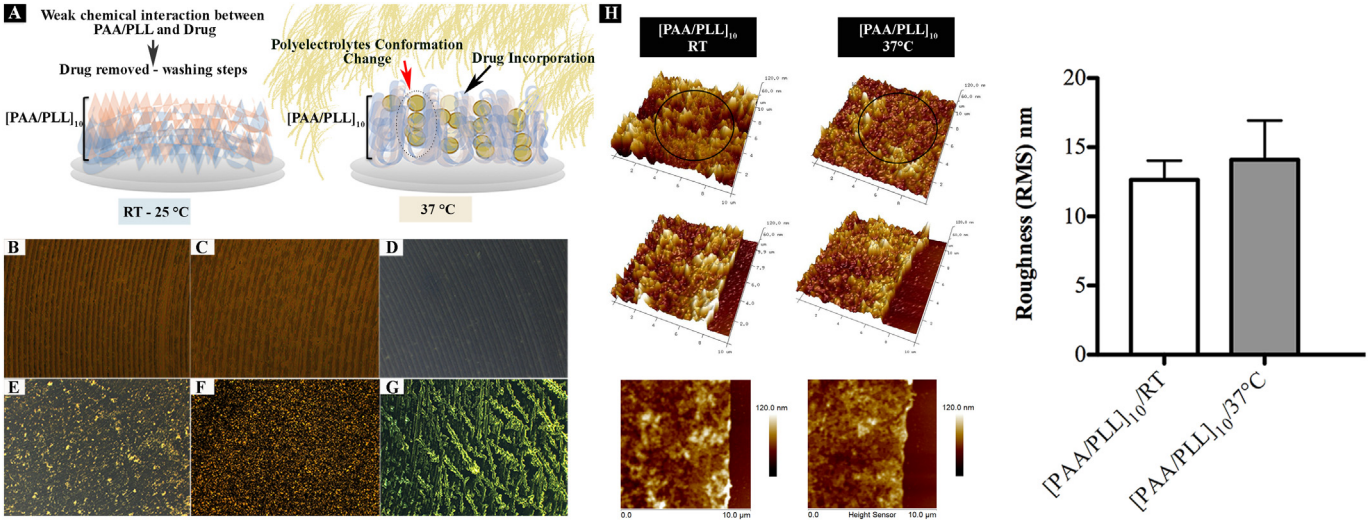

Fig. 6. (A) Schematic illustrating electrolyte conformation change under effect of temperature to drug incorporation. Effect of temperature on TC incorporation into $[PAA/PLL]_{10}$. (B) TC/Ti after 4 days at 37 °C. (C) $[PAA/PLL]_{10}$/TC after 4 days at 37 °C. (D) TC/Ti after 24 h in PBS at 37 °C. (E) $[PAA/PLL]_{10}$ /TC after 24 h in PBS at 37 °C. (F) $[PAA/PLL]_{10}$/TC after 24 h in acetate buffer at 37 °C. (G) $[PAA/PLL]_9$ /TC + $[PAA/PLL]_1$ after 24 h in PBS at 37 °C. (H) Effect of temperature on roughness of $[PAA/PLL]_{10}$ on Ti coated Si (gray bar, $[PAA/PLL]_{10}$/37 °C) in comparison to $[PAA/PLL]_{10}$ (white bar, $[PAA/PLL]_{10}$/RT). Data are shown as mean ± SD. Statistically significant differences are indicated as: $p < 0.05$ (*$p = 0.48$).

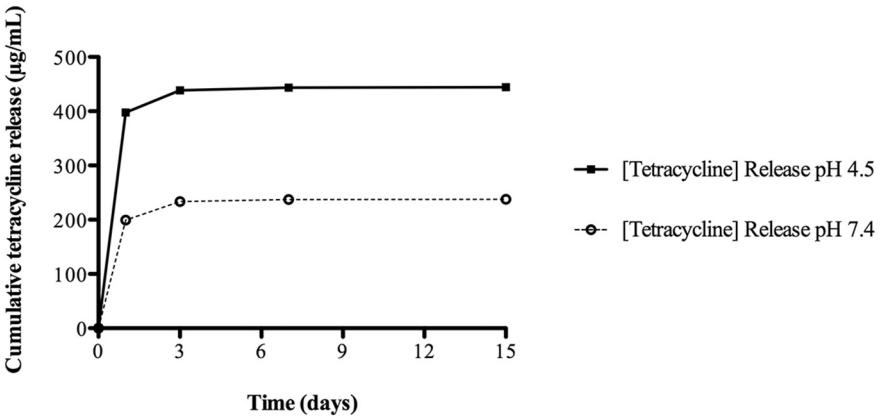

Fig. 7. Cumulative release of TC profile in PBS (pH 7.4) and acetate buffer (pH 4.5). Data represent the mean ± SD (n = 3).

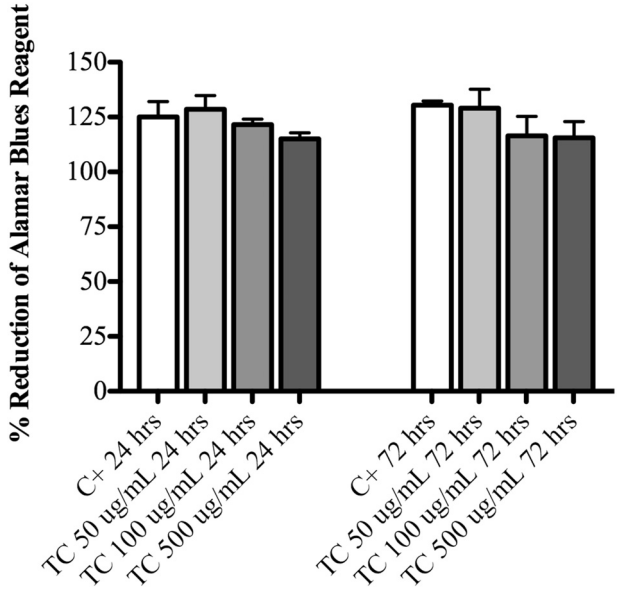

Fig. 8. Effect of TC on HaCat cell viability at 24 and 72 h culture via quantitative measurement of alamar blue staining as indicator of cell viability on tissue culture polystyrene (white bar, C+). Data are shown as mean ± SD; Statistically significant differences are indicated as: $p < 0.05$ (24 h $p = 0.1952$; 72 h $p = 0.2073$).

last double layers construction ([PAA/PLL]$_9$/TC [PAA/PLL]$_1$). [PAA/PLL]$_{10}$/TC coating Ti discs were then evaluated after 24 h immersed in PBS and consistent images revealed the presence of abundant TC fluorescence (Fig. 6G).

Polyelectrolyte multilayers can dehydrate under high temperature and change their conformation [56,57]. This effect seems clear when we compared the pristine coating profile and thickness at room temperature to that after incubation at 37 °C for 24 h. Coatings prepared at room temperature revealed more spread out domains (black circle) than the same coatings kept at 37 °C (Fig. 6H). On the other hand, temperature did not affect coating surface topography.

3.4. TC release in different pH conditions

We determined the release of TC loaded into the coatings over time by HPLC in the supernatant after [PAA/PLL]$_{10}$/TC incubation in PBS (pH = 7.4) and acetate buffer (pH = 4.5), at 37 °C. A concentration of 50 µg/mL served as our limit value to establish the MBC of TC able toward *P. gingivalis*. A burst release of TC from coating was observed under both pH conditions in the first 24 h (Fig. 7). However, a pH-dependent 2-folds increase in TC release was observed for [PAA/PLL]$_{10}$/TC coatings incubated at pH = 4.5 (Fig. 7).

LbL-coatings are temperature and pH sensitive, which means that the polyelectrolytes may adopt some degree of secondary conformational order upon changes in the local pH and ionic strength environment that affect drug release [54,58]. In addition, the ionization degree of polyelectrolytes used for LbL build-up interferes with the stability of the coating due to secondary interactions (hydrogen bonds) and intermolecular associations. As mentioned above, a PLL-terminated coating was defined due to its higher stability under physiologic conditions (pH = 7.4) compared to PAA [58]. However, the pH decrease from 7.4 to 4.5 may affect the molecular arrangement and increase the degree of conformational order upon adsorption [58,59]. At acidic conditions, PLL in the multilayered coating has been found fully protonated, whereas at neutral pH PLL is only partially protonated [58]. In concordance with Prokopovic et al., we assume that the TC release mechanism is related to PLL chain mobility after ionization [49]. Indeed, TC diffusion seems to depend on diffusion of PLL and this supports our assumption that the overall decrease in TC release at pH = 7.4 was affected by stable conformation of PLL. This chemical property may have contributed to rather fast TC release out of the LbL coatings, a convenient perspective to clinical cases where disease is already has been established. In spite of a significant reduction of TC burst release, sustained TC release was observed from coatings up till 15 days of incubation in both pH conditions.

For cytotoxic evaluation, we measured cell viability in different TC concentrations. Since our HPLC data revealed a TC burst release of approximately 400 µg/mL in acidic medium, we investigated whether a concentration up to 500 µg/mL could affect the mammalian cell metabolism. Our data demonstrated that no TC concentration evaluated was capable of interfering in HaCat cell viability even after 72 h of incubation (Fig. 8).

3.5. [PAA/PLL]$_{10}$/TC antimicrobial activity against P. gingivalis W83

In contrast to the potential microbial resistance provoked by systemic administration of antibiotics, local administration minimizes systemic uptake maintaining high levels in the crevicular fluid in periodontal infections [60]. Hence, we investigated if TC released over time would affect *P. gingivalis* accumulation on [PAA/PLL]$_{10}$/TC coated Ti discs. Among a wide-ranging of antimicrobial agents, TC has been clinically used to disinfect contaminated implant surfaces [61,62] due to its activity against a wide range of bacteria in the oral cavity [63,64]. Interestingly, coatings without TC already negatively influenced bacterial adhesion. A significant decrease in bacterial viability on coated versus uncoated Ti discs was observed, with a further reduction of *P. gingivalis* colonies to 2.1 ^{10}Log compared to Ti controls and 4.3 ^{10}Log to positive controls (polystyrene well surface), respectively. The anti-

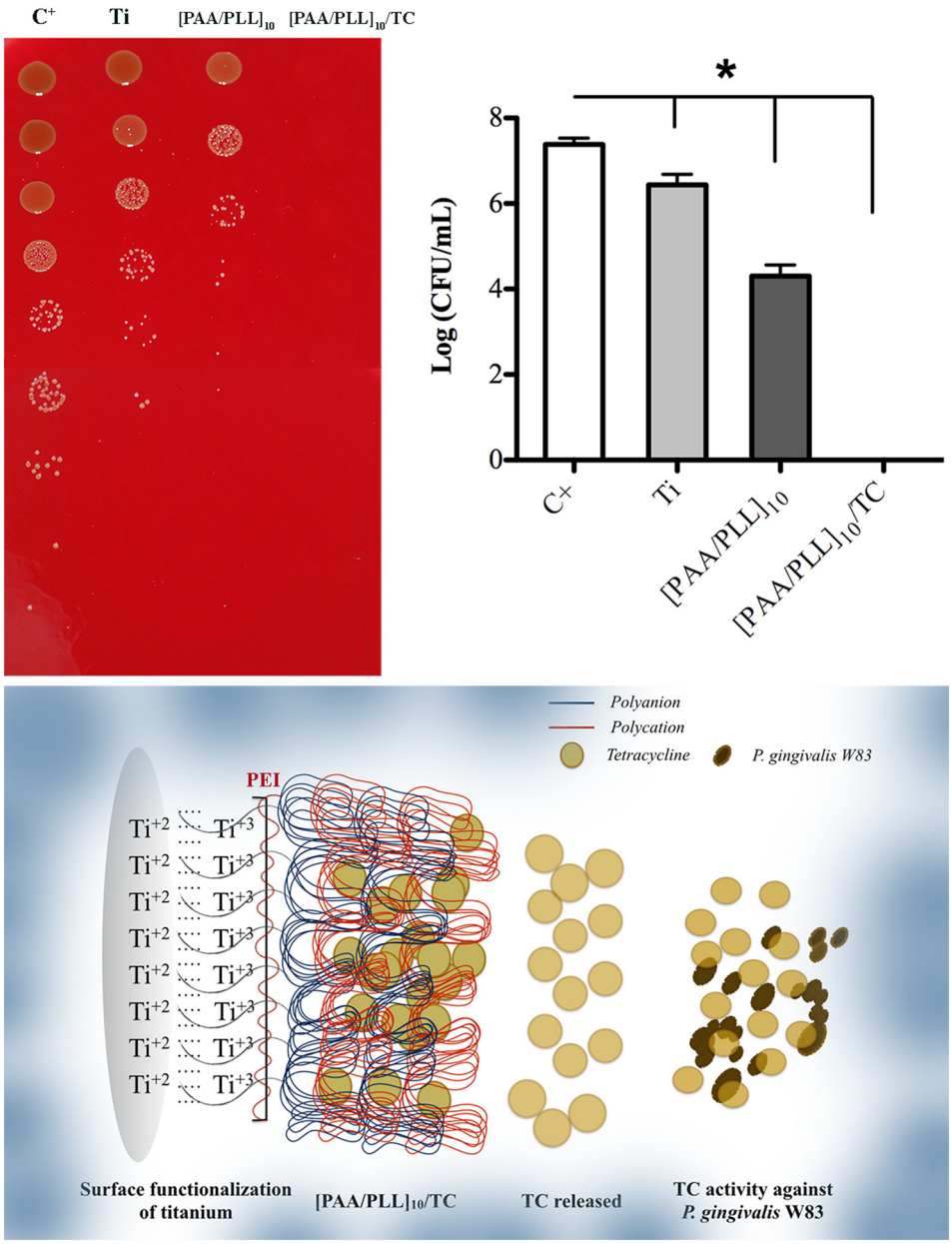

Fig. 9. Quantitative measurement of Log/CFU/mL showing *P. gingivalis* W83 accumulation on uncoated Ti (light gray bar, Ti), significant reduction of number of colonies on $[PAA/PLL]_{10}$ (dark gray bar) and no viable colony on $[PAA/PLL]_{10}$/TC coating Ti discs. Data are shown as the mean ± SD. Statistically significant differences are indicated as: $p < 0.05$ (*$p < 0.0001$).

bacterial effect of the coatings suggests a toxic effect by the presence of acidic functional groups from PAA after PAA dissociation under temperature and pH change [65]. Antimicrobial activity was evaluated after coated and uncoated Ti discs incubation at 37 °C for 48 h. As demonstrated above (see Sections 3.3–3.4), temperature at 37 °C can interfere with the conformation of polyelectrolytes, which means that deprotonated carboxyl groups would lead to a repulsive effect on negative charge from *P. gingivalis* cell wall [66,67]. Since release amounts of TC were higher than the MBC, a strong antibacterial effect was expected. The number of viable bacteria cells was estimated and CFU/mL method recorded no *P. gingivalis* colony on $[PAA/PLL]_{10}$/TC coating Ti discs (Fig. 9). This result points toward an applicable coating capable to release an appropriate dose of TC to diminish *P. gingivalis* colonies.

3.6. Coating as a biomaterial

Our next goal was to evaluate whether coatings had any influence on mammalian cell viability. Alamar Blue testing among coated and uncoated Ti discs, and positive control (cells cultured on polystyrene well surface) showed comparable cell viability of human keratinocytes up to 72 h of culture (Fig. 10A). Similarly, a live/dead assay (Fig. 10B) confirmed retained cell membrane integrity and illustrates morphologically similar cell growth on both coated and uncoated Ti discs. As such, our data corroborate the confirmed biocompatibility of PAA and PLL as polyelectrolyte multilayers used as drug release matrices for biomedical applications [30,68]. However, to the best of our knowledge, this study reports for the first time a successful antibacterial drug delivery approach using PAA and PLL as key components for releasing matrices construction.

4. Conclusion

An effective surgical antibacterial coating was developed by LbL assembly on Ti using tetracycline as an antibiotic drug. Alternating

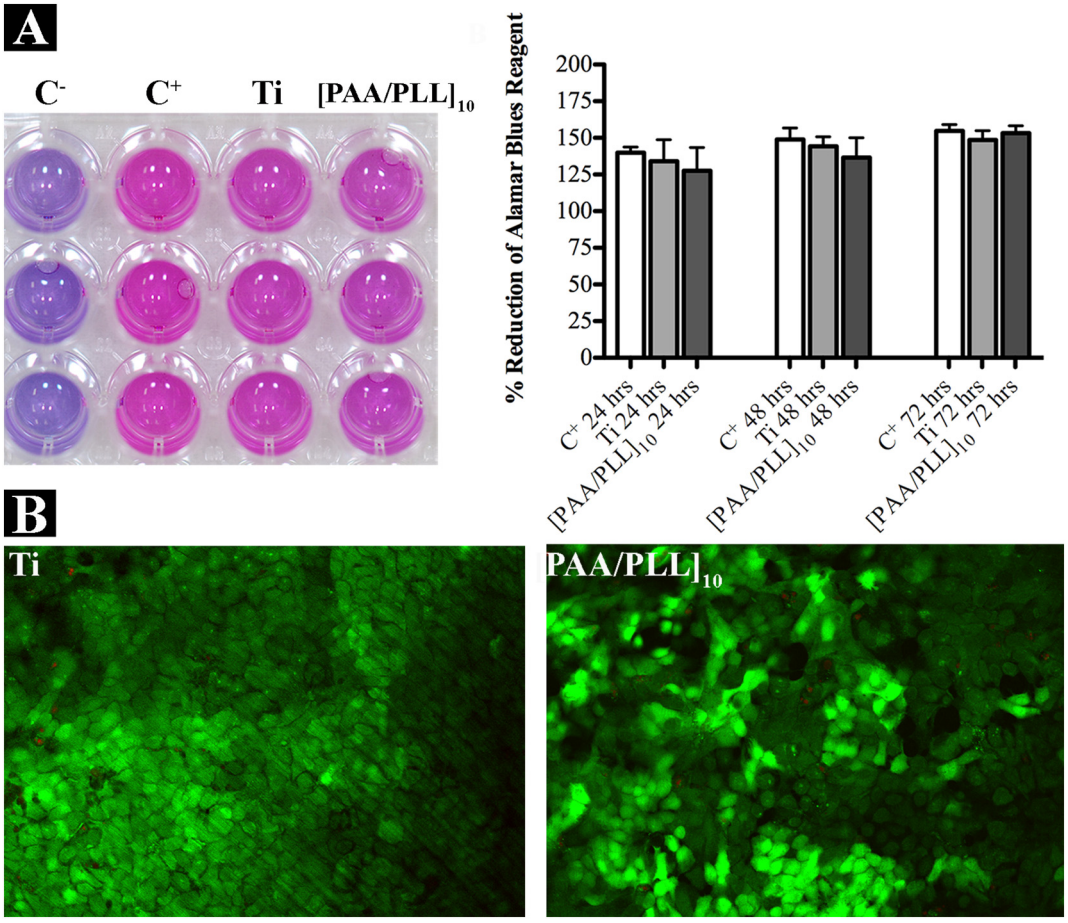

Fig. 10. (A) Effect of $[PAA/PLL]_{10}$ on HaCat cell viability at 24, 48 and 72 h culture via quantitative measurement of alamar blue staining as indicator of cell viability on tissue culture polystyrene (white bar, C+), uncoated Ti discs (light gray bar, Ti) and $[PAA/PLL]_{10}$ coatings on Ti disc (dark gray bar, to $[PAA/PLL]_{10}$). Data are shown as mean ± SD; Statistically significant differences are indicated as: $p < 0.05$ (24 h $p = 0.2766$; 48 h $p = 0.124$; 72 h $p = 0.1532$) (B) Effect of $[PAA/PLL]_{10}$ on HaCat cell viability after 3 days of culture via live/dead analysis (green for live cells, red for dead cells).

polyelectrolyte layers of PAA and PLL showed a stable LbL build-up on Ti, with no cytotoxic effects against human keratinocytes. $[PAA/PLL]_{10}$/TC showed a large tetracycline burst release within 24 h of incubation in both acidic and neutral conditions, with a significant higher release under acidic conditions. Antibacterial effect of $[PAA/PLL]_{10}$/TC was confirmed against *P. gingivalis*, with no viable bacterial remaining after 5 days. This novel drug-delivery system approach holds promise as a facile antibacterial surface modification for metallic percutaneous medical devices.

Declaration of Competing Interest

The authors declare no competing financial interest.

Acknowledgements

Erica Dorigatti de Avila was supported by The São Paulo Research Foundation (FAPESP) grant # 2016/19650-3 and 2015/03567-7. Work at ACTA was supported in part by the UvA Focal Point on Oral Infection and Inflammation. The authors acknowledge the practical assistance of Mrs. CJ Bosch-Tijhof.

References

[1] J. Donne, S. Dewilde, The challenging world of biofilm physiology, Adv. Microb. Physiol. 67 (2015) 235–292.
[2] J.D. Bryers, Medical biofilms, Biotechnol. Bioeng. 100 (2008) 1–18.
[3] D.M. Daubert, B.F. Weinstein, S. Bordin, B.G. Leroux, T.F. Flemming, Prevalence and predictive factors for peri-implant disease and implant failure: a cross-sectional analysis, J. Periodontol. 86 (2015) 337–347.
[4] P.S. Stewart, M.J. Franklin, Physiological heterogeneity in biofilms, Nat Rev Microbiol 6 (2008) 199–210.
[5] A. Amano, I. Nakagawa, S. Hamada, Studying initial phase of biofilm formation: molecular interaction of host proteins and bacterial surface components, Methods Enzymol. 310 (1999) 501–513.
[6] K. Lewis, Riddle of biofilm resistance, Antimicrob. Agents Chemother. 45 (2001) 999–1007.
[7] N.U. Zitzmann, T. Berglundh, Definition and prevalence of peri-implant diseases, J. Clin. Periodontol. 35 (2008) 286–291.
[8] G.E. Salvi, R. Cosgarea, A. Sculean, Prevalence and mechanisms of Peri-implant diseases, J. Dent. Res. 96 (2017) 31–37.
[9] W.J. Loesche, Association of the oral flora with important medical diseases, Curr Opin Periodontol 4 (1997) 21–28.
[10] X. Li, K.M. Kolltveit, L. Tronstad, I. Olsen, Systemic diseases caused by oral infection, Clin. Microbiol. Rev. 13 (2000) 547–558.
[11] K. Kriebel, C. Hieke, B. Muller-Hilke, M. Nakata, B. Kreikemeyer, Oral biofilms from symbiotic to pathogenic interactions and associated disease -connection of periodontitis and rheumatic arthritis by Peptidylarginine deiminase, Front. Microbiol. 9 (2018) 53.
[12] E.D. de Avila, M.J. Avila-Campos, C.E. Vergani, D.M. Spolidorio, A. Mollo Fde, Jr., Structural and quantitative analysis of a mature anaerobic biofilm on different implant abutment surfaces, J. Prosthet. Dent., 115 (2016) 428–436.
[13] E.D. de Avila, R.S. de Molon, B.P. Lima, R. Lux, W. Shi, M.J. Junior, D.M. Spolidorio, C.E. Vergani, F. de Assis Mollo Junior, Impact of physical chemical characteristics of abutment implant surfaces on Bacteria adhesion, J Oral Implantol 42 (2016) 153–158.
[14] E.D. de Avila, B.P. Lima, T. Sekiya, Y. Torii, T. Ogawa, W. Shi, R. Lux, Effect of UV-photofunctionalization on oral bacterial attachment and biofilm formation to titanium implant material, Biomaterials 67 (2015) 84–92.
[15] E.D. de Avila, C.E. Vergani, F.A. Mollo Junior, M.J. Junior, W. Shi, R. Lux, Effect of titanium and zirconia dental implant abutments on a cultivable polymicrobial saliva community, J. Prosthet. Dent. 118 (2017) 481–487.
[16] E.D. de Avila, R.S. de Molon RS, C.E. Vergani CE, F.A. Mollo Jr, V. Salih, The

relationship between biofilm and physical-chemical properties of implant abutment materials for successful dental implants, Materials 7 (2014) 3651–3662.
[17] E.D. de Avila, R.S. de Molon RS, D.M.P. Spolidorio, F.A. Mollo Jr, Implications of Surface and Bulk Properties of Abutment Implants and Their Degradation in the Health of Periodontal Tissue, Materials 18 (2013) 5951–5966.
[18] I.S. Yeo, Reality of dental implant surface modification: a short literature review, Open Biomed Eng J 8 (2014) 114–119.
[19] C.T. Lo, P.R. Van Tassel, W.M. Saltzman, Poly(lactide-co-glycolide) nanoparticle assembly for highly efficient delivery of potent therapeutic agents from medical devices, Biomaterials 31 (2010) 3631–3642.
[20] S. Qayyum, M. Oves, A.U. Khan, Obliteration of bacterial growth and biofilm through ROS generation by facilely synthesized green silver nanoparticles, PLoS One 12 (2017) e0181363.
[21] C. Takahashi, N. Matsubara, Y. Akachi, N. Ogawa, G. Kalita, T. Asaka, M. Tanemura, Y. Kawashima, H. Yamamoto, Visualization of silver-decorated poly (DL-lactide-co-glycolide) nanoparticles and their efficacy against Staphylococcus epidermidis, Mater. Sci. Eng. C Mater. Biol. Appl. 72 (2017) 143–149.
[22] R. Foldbjerg, E.S. Irving, Y. Hayashi, D.S. Sutherland, K. Thorsen, H. Autrup, C. Beer, Global gene expression profiling of human lung epithelial cells after exposure to nanosilver, Toxicol. Sci. 130 (2012) 145–157.
[23] S. Hackenberg, A. Scherzed, M. Kessler, S. Hummel, A. Technau, K. Froelich, C. Ginzkey, C. Koehler, R. Hagen, N. Kleinsasser, Silver nanoparticles: evaluation of DNA damage, toxicity and functional impairment in human mesenchymal stem cells, Toxicol. Lett. 201 (2011) 27–33.
[24] S. Kim, D.Y. Ryu, Silver nanoparticle-induced oxidative stress, genotoxicity and apoptosis in cultured cells and animal tissues, J. Appl. Toxicol. 33 (2013) 78–89.
[25] A.G. Ashbaugh, X. Jiang, J. Zheng, A.S. Tsai, W.S. Kim, J.M. Thompson, R.J. Miller, J.H. Shahbazian, Y. Wang, C.A. Dillen, A.A. Ordonez, Y.S. Chang, S.K. Jain, L.C. Jones, R.S. Sterling, H.Q. Mao, L.S. Miller, Polymeric nanofiber coating with tunable combinatorial antibiotic delivery prevents biofilm-associated infection in vivo, Proc. Natl. Acad. Sci. U. S. A., DOI https://doi.org/10.1073/pnas.1613722113(2016).
[26] J. Poorvashree, D. Suneela, Novel drug delivery of dual acting prodrugs of hydroxychloroquine with aryl acetic acid NSAIDs: design, kinetics and pharmacological study, Drug Deliv Transl Res 7 (2017) 709–730.
[27] K.E. Stott, W.W. Hope, Therapeutic drug monitoring for invasive mould infections and disease: pharmacokinetic and pharmacodynamic considerations, J. Antimicrob. Chemother. 72 (2017) i12–i18.
[28] S. Anandhakumar, A.M. Raichur, Polyelectrolyte/silver nanocomposite multilayer films as multifunctional thin film platforms for remote activated protein and drug delivery, Acta Biomater. 9 (2013) 8864–8874.
[29] I.S. Elizarova, P.F. Luckham, Fabrication of polyelectrolyte multilayered nanocapsules using a continuous layer-by-layer approach, J. Colloid Interface Sci. 470 (2016) 92–99.
[30] S.Y. Wong, J.S. Moskowitz, J. Veselinovic, R.A. Rosario, K. Timachova, M.R. Blaisse, R.C. Fuller, A.M. Klibanov, P.T. Hammond, Dual functional polyelectrolyte multilayer coatings for implants: permanent microbicidal base with controlled release of therapeutic agents, J. Am. Chem. Soc. 132 (2010) 17840–17848.
[31] T. Boudou, T. Crouzier, K. Ren, G. Blin, C. Picart, Multiple functionalities of polyelectrolyte multilayer films: new biomedical applications, Adv. Mater. 22 (2010) 441–467.
[32] H.F. Chuang, R.C. Smith, P.T. Hammond, Polyelectrolyte multilayers for tunable release of antibiotics, Biomacromolecules 9 (2008) 1660–1668.
[33] J. Seo, J.L. Lutkenhaus, J. Kim, P.T. Hammond, K. Char, Effect of the layer-by-layer (LbL) deposition method on the surface morphology and wetting behavior of hydrophobically modified PEO and PAA LbL films, Langmuir 24 (2008) 7995–8000.
[34] N. Takahashi, K. Saito, C.F. Schachtele, T. Yamada, Acid tolerance and acid-neutralizing activity of Porphyromonas gingivalis, Prevotella intermedia and fusobacterium nucleatum, Oral Microbiol. Immunol. 12 (1997) 323–328.
[35] N. Takahashi, C.F. Schachtele, Effect of pH on the growth and proteolytic activity of Porphyromonas gingivalis and Bacteroides intermedius, J. Dent. Res. 69 (1990) 1266–1269.
[36] J.J. van den Beucken, M.R. Vos, P.C. Thune, T. Hayakawa, T. Fukushima, Y. Okahata, X.F. Walboomers, N.A. Sommerdijk, R.J. Nolte, J.A. Jansen, Fabrication, characterization, and biological assessment of multilayered DNA-coatings for biomaterial purposes, Biomaterials 27 (2006) 691–701.
[37] A. Henningsen, R. Smeets, P. Hartjen, O. Heinrich, R. Heuberger, M. Heiland, C. Precht, C. Cacaci, Photofunctionalization and non-thermal plasma activation of titanium surfaces, Clin. Oral Investig. (2017), https://doi.org/10.1007/s00784-017-2186-z.
[38] V.O. De Haan, J. De Blois, P. Van der Ende, H. Fredrikze, A. Van Der Graaf, M.N. Schipper, A.A. Van Well, J. Van Der Zanden, ROG, the neutron reflectometer at IRI, Methods in Phys. Res. A 362 (1995) 19.
[39] L.J. Bannenberg, H. Schreuders, L. van Eijck, J.R. Heringa, N.J. Steinke, R. Dalgliesh, F. Mulder, B. Dam, A.A. van Well, Impact of Nanostructuring on the phase behavior of insertion materials: the hydrogenation kinetics of a magnesium thin film. J. Phys. Chem. 120 7.
[40] R. Cristofoletti, J.B. Dressman, Dissolution methods to increasing discriminatory power of in vitro dissolution testing for ibuprofen free acid and its salts, J. Pharm. Sci. 106 (2017) 92–99.
[41] L.J. Tavares, M.I. Klein, B.H.D. Panariello, E.D. de Avila, A.C. Pavarina, An in vitro model of Fusobacterium nucleatum and Porphyromonas gingivalis in single-and dual-species biofilms, Journal of Periodontal and Implant Science 48 (2018) 12–21.
[42] R. Hayashi, T. Ueno, S. Migita, Y. Tsutsumi, H. Doi, T. Ogawa, T. Hanawa, N. Wakabayashi, Hydrocarbon deposition attenuates osteoblast activity on titanium, J. Dent. Res. 93 (2014) 698–703.
[43] M. Takeuchi, K. Sakamoto, G. Martra, S. Coluccia, M. Anpo, Mechanism of photo-induced superhydrophilicity on the TiO2 photocatalyst surface, J. Phys. Chem. B 109 (2005) 15422–15428.
[44] S.K. Tripathi, Z. Ahmadi, K.C. Gupta, P. Kumar, Polyethylenimine-polyacrylic acid nanocomposites: type of bonding does influence the gene transfer efficacy and cytotoxicity, Colloids Surf B Biointerfaces 140 (2016) 117–120.
[45] S. Yamanlar, S. Sant, T. Boudou, C. Picart, A. Khademhosseini, Surface functionalization of hyaluronic acid hydrogels by polyelectrolyte multilayer films, Biomaterials 32 (2011) 5590–5599.
[46] C.M. Bollen, P. Lambrechts, M. Quirynen, Comparison of surface roughness of oral hard materials to the threshold surface roughness for bacterial plaque retention: a review of the literature, Dent. Mater. 13 (1997) 258–269.
[47] C.M. Bollen, W. Papaioanno, J. Van Eldere, E. Schepers, M. Quirynen, D. van Steenberghe, The influence of abutment surface roughness on plaque accumulation and peri-implant mucositis, Clin. Oral Implants Res. 7 (1996) 201–211.
[48] L.C. Hsu, J. Fang, D.A. Borca-Tasciuc, R.W. Worobo, C.I. Moraru, Effect of micro- and nanoscale topography on the adhesion of bacterial cells to solid surfaces, Appl. Environ. Microbiol. 79 (2013) 2703–2712.
[49] V.Z. Prokopovic, C. Duschl, D. Volodkin, Hyaluronic acid/poly-l-lysine multilayers as reservoirs for storage and release of small charged molecules, Macromol. Biosci. 15 (2015) 1357–1363.
[50] N. Velk, K. Uhlig, A. Vikulina, C. Duschl, D. Volodkin, Mobility of lysozyme in poly (l-lysine)/hyaluronic acid multilayer films, Colloids Surf B Biointerfaces 147 (2016) 343–350.
[51] P.R. Banks, D.M. Paquette, Comparison of three common amine reactive fluorescent probes used for conjugation to biomolecules by capillary zone electrophoresis, Bioconjug. Chem. 6 (1995) 447–458.
[52] M.J. Kutyla, M.W. Boehm, J.R. Stokes, P.N. Shaw, N.M. Davies, R.P. McGeary, J. Tuke, B.P. Ross, Cyclodextrin-crosslinked poly(acrylic acid): adhesion and controlled release of diflunisal and fluconazole from solid dosage forms, AAPS PharmSciTech 14 (2013) 301–311.
[53] R.F. Wong JE, P. Hänni, M. Tanaka, R.V. Klitzing, Swelling behavior of polyelectrolyte multilayers in saturated water vapor, Macromolecules 37 (2004) 7285–7289.
[54] D. Schmaljohann, Thermo- and pH-responsive polymers in drug delivery, Adv. Drug Deliv. Rev. 58 (2006) 1655–1670.
[55] R.G. Thorne, A. Lakkaraju, E. Rodriguez-Boulan, C. Nicholson, In vivo diffusion of lactoferrin in brain extracellular space is regulated by interactions with heparan sulfate, Proc. Natl. Acad. Sci. U. S. A. 105 (2008) 8416–8421.
[56] S.R. MacEwan, D.J. Callahan, A. Chilkoti, Stimulus-responsive macromolecules and nanoparticles for cancer drug delivery, Nanomedicine (Lond) 5 (2010) 793–806.
[57] P. Bawa, V. Pillay, Y.E. Choonara, L.C. du Toit, Stimuli-responsive polymers and their applications in drug delivery, Biomed. Mater. 4 (2009) 022001.
[58] L. Shen, P. Chaudouet, J. Ji, C. Picart, pH-amplified multilayer films based on hyaluronan: influence of HA molecular weight and concentration on film growth and stability, Biomacromolecules 12 (2011) 1322–1331.
[59] S.E. Burke, C.J. Barrett, pH-responsive properties of multilayered poly(L-lysine)/hyaluronic acid surfaces, Biomacromolecules 4 (2003) 1773–1783.
[60] R.D. Finkelman, A.M. Polson, Evidence-based considerations for the clinical use of locally delivered, controlled-release antimicrobials in periodontal therapy, J. Dent. Hyg. 87 (2013) 249–264.
[61] G. La Monaca, N. Pranno, S. Annibali, M.P. Cristalli, A. Polimeni, Clinical and radiographic outcomes of a surgical reconstructive approach in the treatment of peri-implantitis lesions: a 5-year prospective case series, Clin. Oral Implants Res. 29 (2018) 1025–1037.
[62] U.D. Ramos, F. Suaid, U.M.E. Wikesjo, C. Susin, P.C. Vital, S.L.S. de Souza, M.R. Messora, D.B. Palioto, A.B. Novaes, Jr., Microbiologic effect of two topical anti-infective treatments on ligature-induced peri-implantitis: a pilot study in dogs, J. Periodontol., 89 (2018) 995–1002.
[63] A.D. Haffajee, S.S. Socransky, J.C. Gunsolley, Systemic anti-infective periodontal therapy. A systematic review, Ann Periodontol 8 (2003) 115–181.
[64] P. Matesanz-Perez, M. Garcia-Gargallo, E. Figuero, A. Bascones-Martinez, M. Sanz, D. Herrera, A systematic review on the effects of local antimicrobials as adjuncts to subgingival debridement, compared with subgingival debridement alone, in the treatment of chronic periodontitis, J. Clin. Periodontol. 40 (2013) 227–241.
[65] G. Gratzl, C. Paulik, S. Hild, J.P. Guggenbichler, M. Lackner, Antimicrobial activity of poly(acrylic acid) block copolymers, Mater. Sci. Eng. C Mater. Biol. Appl. 38 (2014) 94–100.
[66] J. Santiago-Morales, G. Amariei, P. Leton, R. Rosal, Antimicrobial activity of poly (vinyl alcohol)-poly(acrylic acid) electrospun nanofibers, Colloids Surf B Biointerfaces 146 (2016) 144–151.
[67] M.M. Cowan, H.C. van der Mei, P.G. Rouxhet, H.J. Busscher, Physicochemical and structural investigation of the surfaces of some anaerobic subgingival bacteria, Appl. Environ. Microbiol. 58 (1992) 1326–1334.
[68] A. Jaklenec, A.C. Anselmo, J. Hong, A.J. Vegas, M. Kozminsky, R. Langer, P.T. Hammond, D.G. Anderson, High throughput layer-by-layer films for extracting film forming parameters and modulating film interactions with cells, ACS Appl. Mater. Interfaces 8 (2016) 2255–2261.